Polymer Vol. 39 No. 24 pp. 5899–5912, 1998
0032-3861/98/$ – see front matter

PII: S0032-3861(98)00114-1

Rheo-photoacoustic *FT*i.r. and morphology studies of molecular weight–strain dependence in poly(vinylidene fluoride)

Bret W. Ludwig and Marek W. Urban*
Department of Polymers and Coatings, North Dakota State University, Fargo, ND 58105, USA
(Received 12 March 1996; revised 4 April 1997; accepted 2 February 1998)

The influence of molecular weight on the strain-dependent permeability of poly(vinylidene fluoride) (PVDF) is investigated. Permeability measurements were performed on spherulitic and fibrous PVDF at various concentration levels of ethyl acetate (EtAc). Rheo-photoacoustic Fourier transform infrared spectroscopy (RPA *FT*i.r.) was used as a quantitative measure of the desorption diffusion coefficient. Polymer molecular weight, crystallite size and the number of tie molecules in the network have a significant effect on the morphological changes as a result of plastic and elastic deformations. The head-to-head and tail-to-tail defect content also plays a significant role on the mechanism of plastic deformation. By reducing the stability of crystallites, higher defect contents appear to diminish the yield stresses in PVDF which result in transition to the fibrous morphology without void formation. © 1998 Published by Elsevier Science Ltd. All rights reserved.

(Keywords: *FT* i.r.; morphology; poly(vinylidene fluoride)

INTRODUCTION

Owing to the presence of various crystalline structures and their interconversion, poly(vinylidene fluoride) (PVDF) exhibits fairly complex polymorphism behaviour. It can exist in four different crystalline structures[1,2] two of which are most common, and are designated as α and β phases. The α polymorph has an orthorhombic unit cell containing 2 polymer chains in a 2_1 helix conformation[3], and is obtained by cooling PVDF from the melt. This phase can be converted to the β form by drawing it at 25°C[4–6]. The β phase consists of PVDF chains with all *trans* (planar–zigzag) conformations in a monoclinic unit cell[3,6], and exhibits strong piezoelectric properties[7]. The remaining crystalline polymorphs are designated as the γ and δ phases. The polar γ phase is obtained by crystallization at temperatures greater than 150°C, and consists of PVDF chains with T_3GT_3G' conformations in a monoclinic unit cell[8]. The (phase is obtained by poling the (form in electric fields of 1.2 MV cm^{-19}. This phase maintains the same chain conformation and unit cell as the α phase[8].

While the mechanism of transformation from α to β form, resulting from elongation, has been studied by X-ray diffraction and i.r. spectroscopy, the influence of small deformations ($< 20\%$) on the transport properties of PVDF were not considered. In the earlier publications[10–12], we demonstrated the utility of rheo-photoacoustic Fourier transform infrared spectroscopy (RPA *FT*i.r.) to determine the permeability of fluorinated polymer films by organic solvents. Low degrees of uniaxial elongation were shown to result in an increased permeability of PVDF. It was also observed that there is a linear relationship between PVDF's crystallinity and permeability. In an effort to minimize the complicating effects of molecular weight on film morphology, these studies were performed on a single grade of PVDF (150 000 MW). In this study, we expand the scope of the earlier work, and examine the effect of molecular weight on the strain-dependent permeability of semicrystalline PVDF polymers. Because the head-to-head (HH) and tail-to-tail (TT) defects in a polymer backbone can influence the polymer crystallinity[13,14], their role on the stress-induced morphological changes will be also examined.

EXPERIMENTAL

Specimen preparation and spectral measurements

Powdered PVDF samples were obtained from Elf Atochem Inc. and their properties are listed in *Table 1*. Ethyl acetate was acquired from Aldrich Chemical Co., and was used without purification. Films 350 ± 20-μm-thick films were prepared by pressure-moulding of PVDF at 220°C, and cooling it in a mould at a rate of 20°C min^{-1}. Dumbbell shaped samples 75 mm long, end width 14 mm, notch length 25 mm, and notch width 7 mm were cut from prepared films. Fibrous specimens were obtained by drawing dumbbell-shaped samples at 25°C. The specimens were saturated with ethyl acetate (EtAc) by immersing them for a minimum of 72 h and drying for 30, 60 and 120 min in order to determine the effect of initial EtAc content. Samples with a fibrous structure were saturated with EtAc, following transformation to the fibrous form.

As we established earlier[10–12], the utilization of PA *FT*i.r. for monitoring diffusion in polymer films involves placing a diffusant-containing polymer in a photoacoustic cell, covering the specimen with a 'photoacoustic umbrella', and detection of species diffusing out of the specimen. As diffusant molecules migrate through the polymer network to the film surface and evaporate, the concentration of vapours in the photoacoustic cell can be accurately determined. Knowing the amount of EtAc in the gas phase allows us to determine either relative rates of diffusion, or through

* To whom correspondence should be addressed

Table 1 PVDF samples used in this study

Mn[a]	HH–TT defects[b] (mol%)	Crystallinity[c] (± 2%)	Melting point[c] (± 1°C)
45 000	9–10	55	170
59 000	11–12	45	161
150 000	9–10	52	168
350 000	11–12	47	163

[a]Determined by high temperature g.p.c. analysis (supplier)
[b]Determined by solid state ^{19}F n.m.r. (supplier)
[c]Determined by d.s.c. measurements (this lab.)

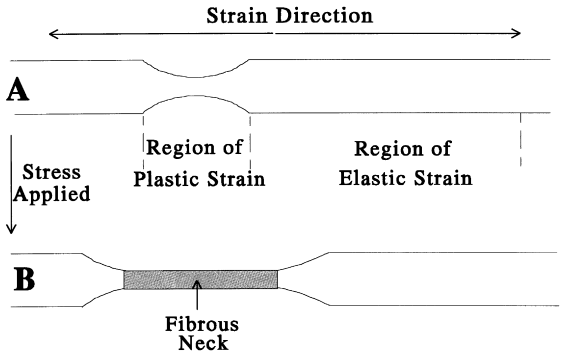

Figure 1 Diagram of sample illustrating deformation upon application of stress: (A) specimen before application of stress; (B) elongated specimen

correlation with independently determined diffusion coefficients, quantitative measure of the desorption diffusion coefficient (D_d). A schematic diagram of the *FT*i.r. set-up was published elsewhere[10]. PA *FT*i.r. spectra, which represent 70 coadded scans ratioed against a carbon black background, were collected on a Mattson Sirius 100 i.r. spectrometer operated at a mirror speed of 0.12 cm s^{-1}. In a similar way to the previous studies[10,11], the integrated intensity of the 1768 cm^{-1} band, attributed to the C=O stretching vibrations of EtAc, was used as a quantitative measure of the amount of solvent present in the vapour phase.

Sample deformation

In an effort to determine the effect of deformation on the transport properties of the plastically and elastically deformed regions, specimens with the shapes shown in *Figure 1* were prepared. As a result of elongation, PVDF forms a 'neck'. This region experiences non-recoverable, plastic deformation, while deformations experienced by other parts of the film are of an elastic nature.

Figure 1A represents a non-deformed sample, whereas *Figure 1B* depicts the film after elongation. In order to examine the effect of plastic deformation on permeability, the sample was loaded into the RPA cell in such a way that the neck was formed within a sealed photoacoustic chamber, allowing analysis within that region. On the other hand, examination of the elastically deformed PVDF regions was conducted by allowing a neck formation outside the cell.

Scanning electron microscopy

Scanning electron micrographs of film surfaces and cross sections were obtained using a JEOL JSM 6300V scanning electron microscope operated at 7 kV. All samples were sputtered with a 60/40 gold/palladium alloy. Micrographs of PVDF sample cross sections were obtained from the edges of samples which had been fractured at liquid N_2 temperature.

Optical microscopy

In an effort to determine the expansion of volume which takes place during the elongation of a PVDF film, the dimensions of a specimen were determined as a function of elongation using an Olympus C-35 AD camera, attached to an Olympus SZH microscope with a magnification of 50 ×.

Differential scanning calorimetry

Differential scanning calorimetry (d.s.c.) measurements were performed on a DuPont Instruments 910 differential scanning calorimeter. Measurements of the enthalpy crystallization and melting point were performed at a heating rate of 10°C min^{-1}. All thermograms were collected from 60 to 220 °C. A value of 22.2 cal g^{-1} was taken as the equilibrium melting enthalpy of the (polymorph of PVDF[15], in calculating the degree of crystallinity from d.s.c. measurements.

Stress–strain measurements

Stress–strain measurements were performed on a MTS SINTECH Q-Test IV mechanical tester. Film dimensions were the same as the dimensions used in the RPA *FT*i.r. spectroscopic studies. The tests were performed using a gauge length of 50 mm and a crosshead speed of 100 mm min^{-1}.

Diffusion coefficient determination

A half-time of desorption, $t_{1/2}$, is defined as the time required for half of the initial weight of the EtAc to evaporate from the polymer specimen. This quantity was determined by measuring a loss of EtAc from saturated films using an analytical balance with a sensitivity of 0.1 mg. Based on these data, the diffusion coefficient was determined using the following relationship[16,17]

$$D_d = 0.05\frac{L^2}{t_{1/2}} \quad (1)$$

where D_d is the desorption diffusion coefficient, L is the sample thickness, and $t_{1/2}$ is the half-time of desorption. The amount of EtAc sorbed by PVDF was obtained by subtracting the weight of a sample from that of the same polymer specimen saturated with EtAc.

RESULTS AND DISCUSSION

Before we examine the effect of elongation of PVDF on its permeability, let us preface our discussion by examining the anticipated influence of molecular weight on film morphology; specifically, crystallite size dependence on molecular weight, formation of intercrystalline tie molecules and overall crystallinity. For a typical thermoplastic polymer, as molecular weight increases, the rate of crystallization[18], number of chain entanglements and tie molecules bridging the amorphous regions also increase[19]. As the rate of crystallization increases with molecular weight, the formation of larger crystallites is anticipated. However, for high molecular weight polymers, an increase in crystallization rate can be offset by chain entanglements, which often interfere with the crystallization process[18,20]. As a result, the maximum rate of crystallization for polyethylene is achieved for molecular weights of approximately 1×10^5. Thus, while the number of tie molecules increases linearly with molecular weight, crystallite size and overall crystallinity increase, up to a molecular weight of approximately 1×10^5. Beyond that point, these relationships are no longer

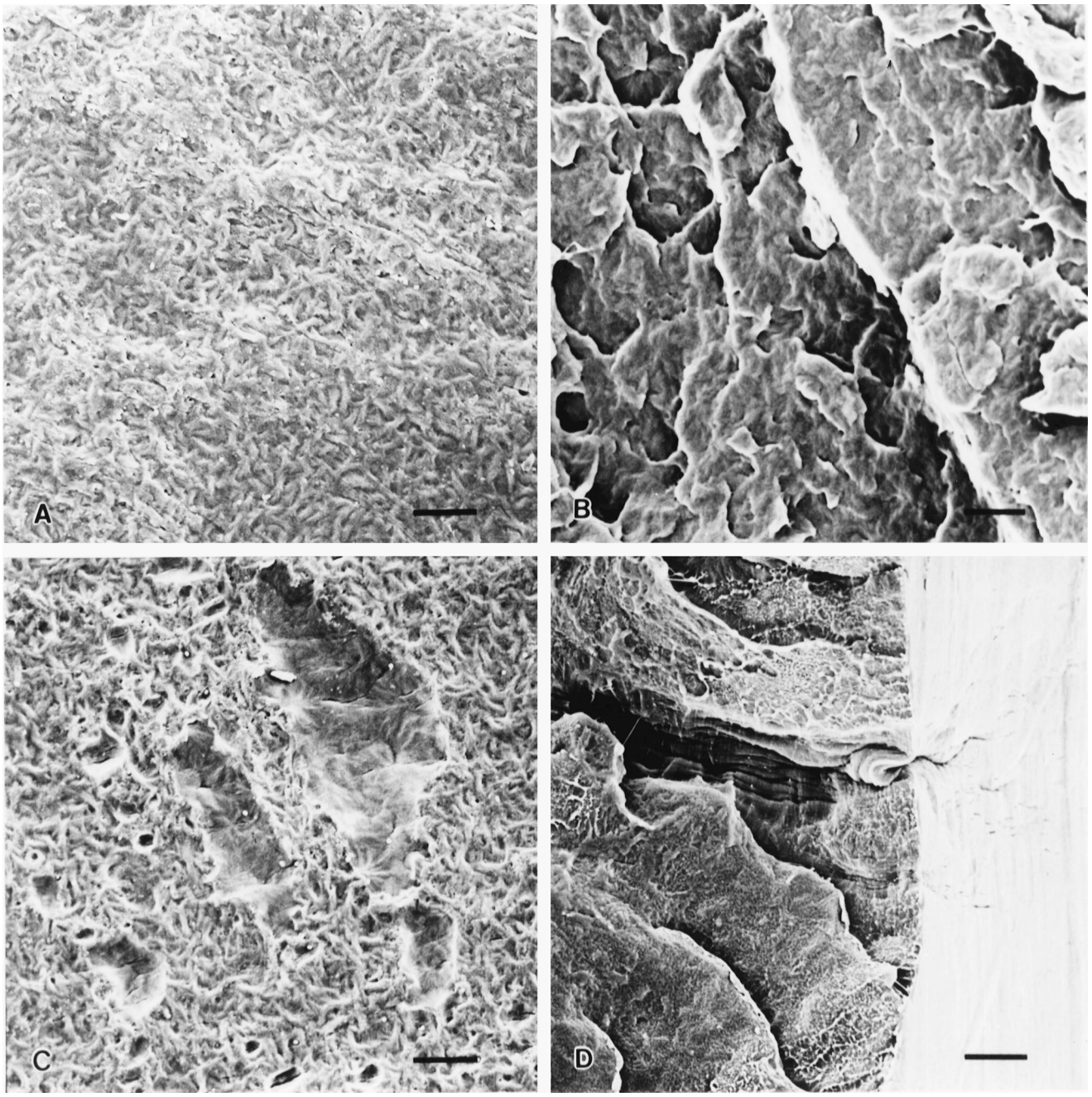

Figure 2 Scanning electron micrographs of 150 000 MW PVDF: (A) film surface, 0% strain; (B) cross section taken near film surface, 0% strain; (C) film surface, 10% local strain; (D) cross section taken near film surface, 10% local strain. The scale bar present in the micrographs represents 5 μm

valid, and typically they decline. If one draws an analogy to PVDF of an equal chain length, PVDF of 2.3×10^5 molecular weight would achieve a maximum rate of crystallization.

With this in mind, let us consider that the crystallite size and transport properties of semicrystalline polymers can be related through the following relation

$$D = \Psi D_a \tag{2}$$

where D is the diffusion coefficient of a semicrystalline polymer, D_a is the diffusion coefficient of an amorphous film of the same material, and Ψ is the tortuosity factor. The value of Ψ is always less than one, and it depends upon the degree of crystallinity, crystallite size and crystallite orientation. The tortuosity factor is a measure of the increased path length that a diffusing molecule must take through a semicrystalline film owing to the impermeability of the crystalline phase. A larger crystallite size results in longer paths for diffusing molecules to reach the film surface, and a smaller value of Ψ. Our interest lies in determining how variations in initial polymer morphology influence permeability changes during deformation.

Although our primary interest is in a quantitative analysis of diffusion, scanning electron microscopy (SEM) enables qualitative observations of morphological changes which may occur during deformation of PVDF, and thus may affect diffusivity. Upon examining the PVDF films by SEM, it was found that the observable structural features at 0% strain are independent of molecular weight. The electron micrographs presented in *Figure 2* are of 150 000 MW PVDF, and represent morphological features resulting from external forces imposed on PVDF. While the micrograph

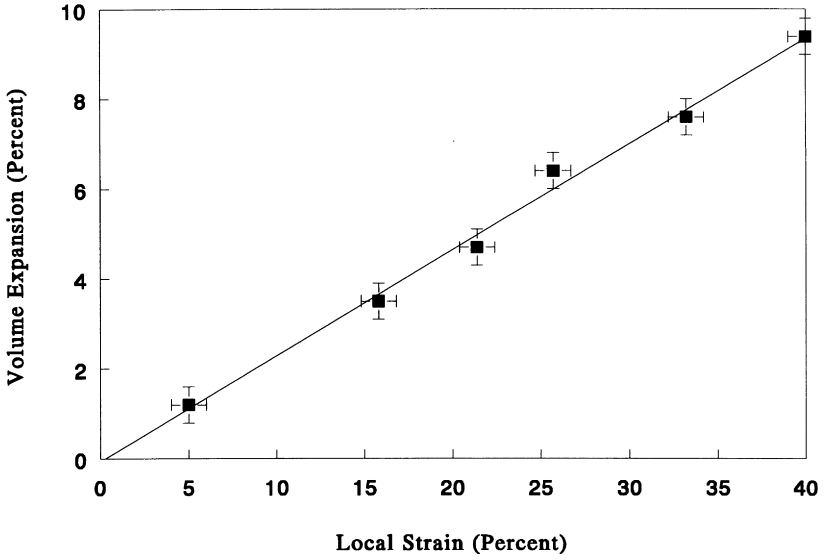

Figure 3 Volume expansion experienced by a 150 000 MW PVDF specimen during elongation

shown in *Figure 2A* illustrates the surface texture, and indicates a random orientation of crystalline entities, the micrograph in *Figure 2B* was taken from the cross section near the film surface, and demonstrates that the textured morphology visible at the film surface is present throughout the film thickness. Thus, the presented micrographs do not represent only a surface phenomenon, but PVDF morphology across the film thickness. The individual 'fibrils' visible on the film surface in *Figure 2A* are between 2000 and 4000 Å thick. While this value is much larger than that of individual PVDF lamellar crystals obtained under similar experimental conditions (approximately 200 Å)[21], the fibrils shown in *Figure 2A* may consist of stacks of lamellae, which have been observed in poly(ethylene)[22].

As the 45 000 and 150 000 MW PVDF specimens are deformed from the original spherulitic morphology to the fibrous form, the originally transparent film takes on a white appearance, especially in the early stages of the transition. In a previous study[10], we had attributed the whitening to microvoid formation, which resulted in a significant increase in the transport properties. Again, *Figure 2C* and D present the surface and the cross-section, respectively, of a specimen which experienced 10% local strain, and exhibited the first signs of whitening. It appears that the microvoids (*Figure 2C*) and the microcracks (*Figure 2D*) occur throughout the cross-section of the film, and are not attributed to a surface phenomena.

While SEM provides visual evidence for morphological changes, which may or may not result in increased permeability, when the spherulitic morphology undergoes transformation to a fibrous form, there are two inherent problems in monitoring morphology–permeability relationships. First, it is difficult to attain a quantitative measure of permeability changes as a function of strain. Second, the morphological changes, which occur during the early deformation stages are too small to be observed without damaging electron-sensitive polymer films. Since rheo-photoacoustic *FT*i.r. studies can provide quantitative measurements of strain-dependent permeabilities[10,12], even at low degrees of strain, we will utilize this approach and combined with the SEM measurements, identify morphological features responsible for the observed trends in diffusion processes.

In addition to the appearance changes, the volume of PVDF films with spherulitic morphology is expected to increase upon elongation owing to crystallites interfering with the lateral contraction of the film. In an effort to demonstrate the volume increase which occurs upon uniaxially elongating a PVDF film, the dimensions of a 150 000 MW specimen were determined by taking measurements from photographs of the film surface and cross section at a series of elongations. These measurement were conducted using an optical microscope. *Figure 3* illustrates that the volume appears to increase linearly with the degree of deformation. This fact, combined with the non-deformable nature of the polymer crystallites, leads one to conclude that the volume, and therefore the free volume, of the amorphous phase of a spherulitic specimen increases with deformation.

Permeability measurements as a function of strain provide useful insights into the morphological changes occurring during the early stages of deformation. In the previous studies[10,11], we utilized ethyl acetate (EtAc) as a molecular probe of permeability. However, when utilizing the rate of exudation of EtAc from PVDF as a measure of permeability, it should be kept in mind that the concentration of EtAc decreases as the experiment proceeds. *Figure 4* demonstrates the variation in the amount of EtAc diffusing from a saturated PVDF sample as a function of time. This curve can be represented by the following relationship

$$PA = A \exp[x(-t^{1/2})] \tag{3}$$

or

$$\ln(PA) = \ln A - xt^{1/2} \tag{3'}$$

where PA is the integrated photoacoustic intensity of the EtAc carbonyl band at 1768 cm^{-1}, t is the time from which the sample was removed from the solvent, A is a pre-exponential term equal to the PA intensity at $t = 0$, and x is the spectroscopically determined diffusion parameter. If equation (3′) indeed describes the diffusion process, plotting the natural log of the photoacoustic intensity *versus* the square root of time one would anticipate obtaining a straight line with a slope of $-x$. *Figure 5* presents the relationship for a series of PVDF samples between the

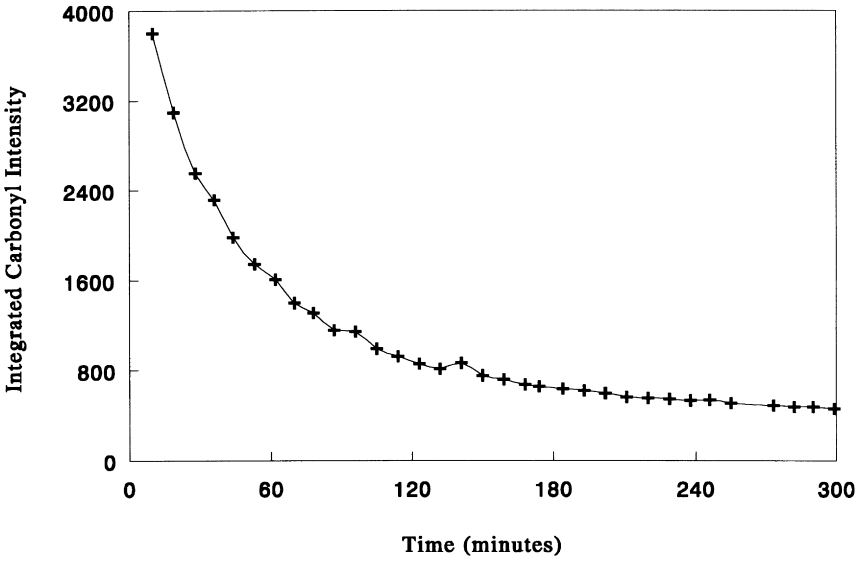

Figure 4 Integrated intensity of the band at 1768 cm^{-1} plotted as a function of time for PVDF saturated with EtAc

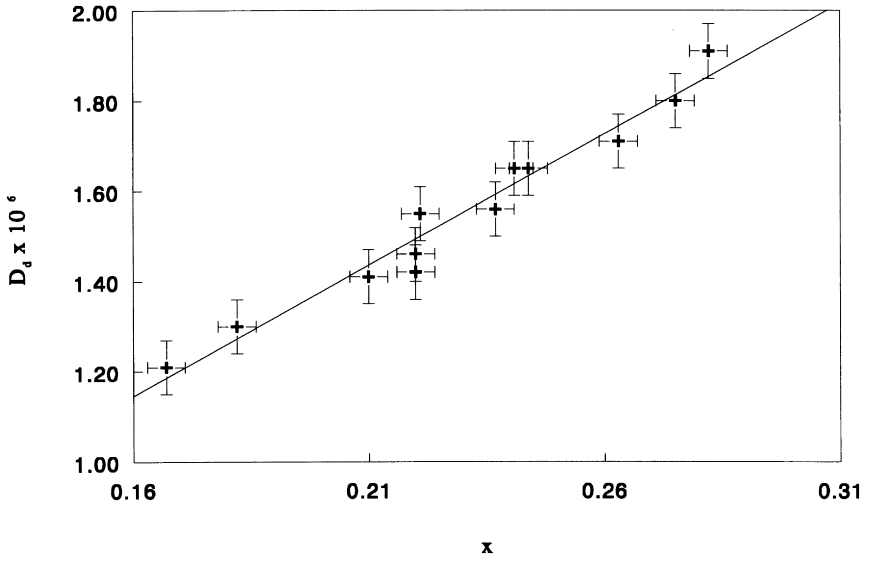

Figure 5 Calibration curve relating the spectroscopically determined diffusion coefficient (x), to the desorption diffusion coefficients (D_d), independently determined for the same samples

spectroscopically determined diffusion parameter (x) and independently measured desorption diffusion coefficients (D_d) determined from equation (1). Such a plot will allow us to measure quantitatively the permeability of polymers under constant imposed strains.

As a first step in examining the permeability of PVDF, quantitative measurements of D_d were performed on PVDF films for each molecular weight under conditions listed in *Table 2*. While D_d of PVDF in the spherulitic form was measured at 0 and 5% elongations, for fibrous PVDF samples, D_d was determined in stress-relaxed films, and under a constant stress.

Before we discuss transport properties of the fibrous PVDF, let us examine the corresponding SEM micrographs, which are presented in *Figure 6*, and depict the fibrous neck region of a 150 000 MW PVDF sample, which experienced local strains greater than 400%. *Figure 6A* presents a cross-sectional view of the film near the film surface, whereas *Figure 6B* and *C* show the surface of fibrous PVDF samples, before and after immersion of the specimens for 72 h in EtAc, respectively. As seen in *Figure 6*, fibres are oriented parallel to the strain direction, which is indicated by the arrows. *Figure 6A* and *B* indicate that prior to the film being immersed in EtAc, a significant fraction of unoccupied volume is present. As seen in *Figure 5C*, the plasticizing action of EtAc enables the fibres to coalesce into a nearly continuous film, causing the opaque, white fibrous sample to become transparent. The coalescence of the fibres enables determination of the transport properties of fibrous PVDF which, in the uncoalesced state, would be dominated by the transport properties of the unoccupied volume. Following coalescence, the application of stress to fibrous PVDF, parallel to the fibre axis, results in the lengthening of the fibrous region through transformation of additional spherulitic material to the fibrous form at the ends of the neck, and not in the separation of the fibres.

Let us now return to the main theme and examine the relationship between polymer morphology and transport

Table 2 Desorption diffusion coefficient (D_d) ($\times 10^6\ cm^2\ min^{-1}$) obtained for various PVDF homopolymer morphologies

MW	Morphology			
	Spherulitic		Fibrous	
	0% Strain	5% Strain	Stress relaxed	Stressed[a]
45 000	1.71 ± 0.03	1.79	1.73	1.50
59 000	1.41	1.51	1.54	1.72
150 000	1.36	1.44	1.31	1.07
350 000	1.48	1.44	1.20	1.13

[a] D_d was measured with a constant stress (≈ 20 N) applied to sample

properties. In the earlier studies[10], we determined that the permeability of as-received PVDF ($M_n = 150\,000$), increased when a spherulitic sample was elongated by 5%. However, the fibrous form exhibited a decreased permeability when a constant stress was applied parallel to the fibre axis. As seen in *Table 2*, the data for the 45 000 and 150 000 MW display trends similar to those observed for the as-received PVDF. The value of D_d increased from $1.71 \times 10^{-6}\ cm^2\ min^{-1}$ and $1.36 \times 10^{-6}\ cm^2\ min^{-1}$ to $1.79 \times 10^{-6}\ cm^2\ min^{-1}$ and $1.44 \times 10^{-6}\ cm^2\ min^{-1}$ upon the 5% deformation of spherulitic 45 000 and 150 000 MW PVDF, respectively. Fibrous 45 000 and 150 000 MW PVDF exhibited decreases in D_d values from 1.73 and 1.31 to 1.50 and 1.07, respectively. The increased permeability, observed on straining spherulitic PVDF, was attributed to the increased free volume created in an amorphous phase, by the interference of crystallites with lateral contraction of the film[9]. In the case of fibrous PVDF morphology, tie molecules are pulled taut, limiting the motion of the amorphous phase material, and thereby decrease its free volume, which accounts for a lower permeability of the fibrous 45 000 and 150 000 MW PVDF films upon application of stresses.

The results presented in *Table 2* also indicate that PVDF specimens with 59 000 and 350 000 MW do not follow the above trends. It appears that PVDF with 350 000 MW exhibits a decreased D_d value from $1.20 \times 10^{-6}\ cm^2\ min^{-1}$ to $1.13 \times 10^{-6}\ cm^2\ min^{-1}$ upon application of stress to the fibrous polymorph. This observation is in agreement with the previous findings[10]. However, as seen in *Table 2*, upon 5% elongation, the specimens with a spherulitic morphology experience a decrease of the D_d values, from $1.48 \times 10^{-6}\ cm^2\ min^{-1}$ to $1.44 \times 10^{-6}\ cm^2\ min^{-1}$. This observation indicates a decrease in the amorphous phase free volume, which is contrary to the behaviour expected for a semicrystalline polymer, in which the free volume is expected to increase as a result of crystallites interfering with the lateral contraction of the film. Since the number of tie molecules in semicrystalline polymers is linearly related to molecular weight, the 350 000 MW PVDF should have a significantly greater number of tie molecules than the other specimens examined. The large number of tie molecules, when pulled taut during elongation, reduces the mobility of the amorphous phase material, and thus counters the effect of volume expansion and permeability decreases.

While elongating spherulitic 59 000 MW PVDF results in the expected increased permeability (D_d equal to $1.41 \times 10^{-6}\ cm^2\ min^{-1}$ and $1.51 \times 10^{-6}\ cm^2\ min^{-1}$ at 0 and 5% deformation, *Table 2*), stresses applied to the fibrous specimens also result in the increased mobility of EtAc within the film. As seen in *Table 2*, this is illustrated by the increase in the D_d values, from 1.54×10^{-6} to $1.72 \times 10^{-6}\ cm^2\ min^{-1}$. Relatively low permeability of the

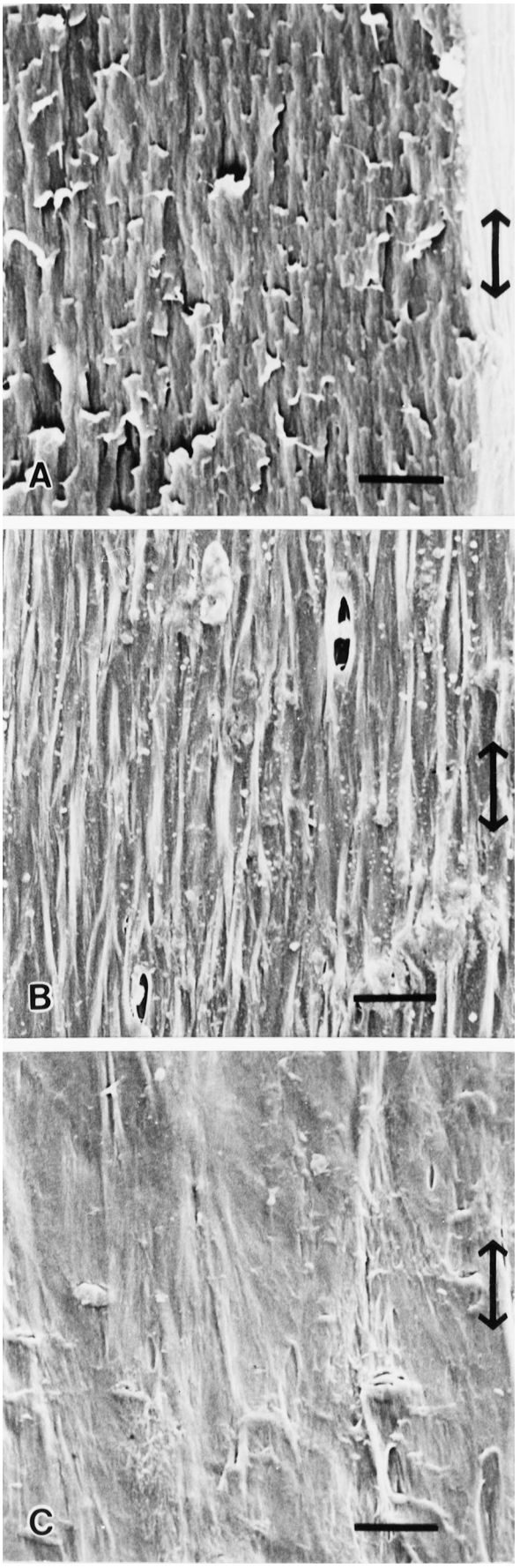

Figure 6 Scanning electron micrographs of 150 000 MW PVDF after experiencing local strains in excess of 400%: (A) cross section taken near film surface; (B) film surface; (C) film surface following immersion in EtAc for 72 h. The scale bar present in the micrographs represents 5 μm

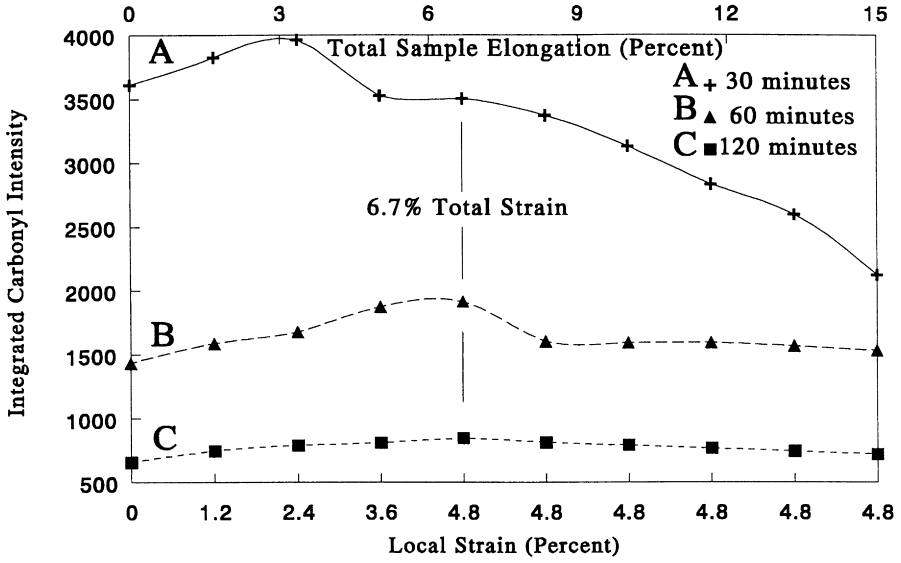

Figure 7 Integrated intensity of the band at 1768 cm^{-1} plotted as a function of elongation. Data obtained from PVDF of 45 000 MW experiencing elastic deformation. Curves A, B and C represent films dried 30, 60 and 120 min prior to elongation, respectively

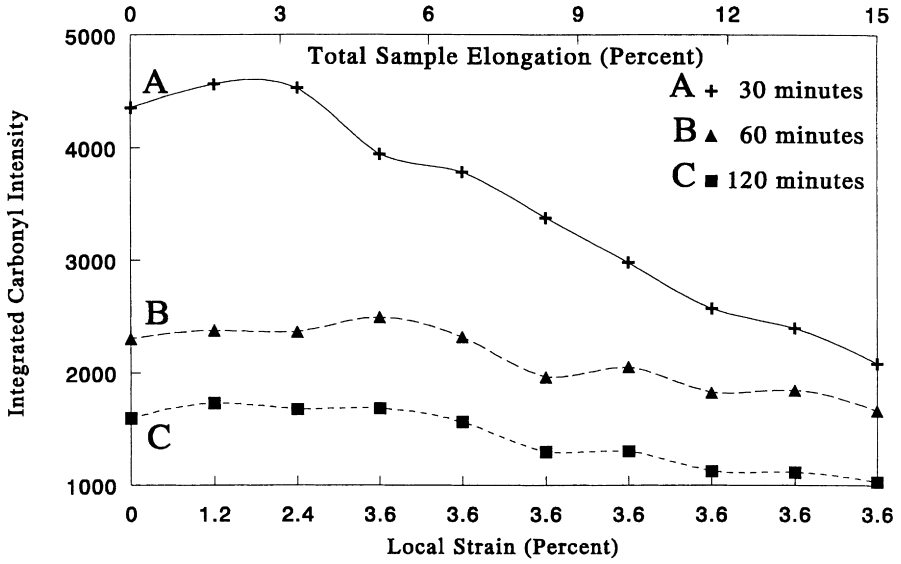

Figure 8 Integrated intensity of the band at 1768 cm^{-1} plotted as a function of elongation. Data obtained from PVDF of 59 000 MW, experiencing elastic deformation. Curves A, B and C represent films dried 30, 60 and 120 min prior to elongation, respectively

spherulitic form, combined with the low crystallinity values obtained by d.s.c. measurements, suggests that large crystallites are the primary morphological features. A combination of large crystallites and low molecular weight would result in few tie molecules bridging the crystals. Upon application of stress to the fibrous polymorph, one would anticipate a disruption of the structure, with insufficient tie molecules to hinder motion of the polymer chains in the amorphous phase.

Given the above insight into the structure of PVDF, let us examine the effect of elastic deformation on PVDF transport properties. As described above, these experiments were performed with the neck of the film formed outside the RPA *FT*i.r. cell sample compartment. Changes of permeability for PVDF samples with MW ranging from 45 000 to 350 000, induced by elastic deformation, are shown in *Figures 7–10*, respectively. The curves in *Figures 7–10* represent the integrated intensity of the carbonyl band at 1768 cm^{-1}, due to vapour phase EtAc, recorded as a function of strain. Curves A, B and C were obtained from the specimens allowed to dry at 25°C for 30, 60 and 120 min, respectively, prior to monitoring the permeability under various strains. Each data point presented in *Figures 7–14* represents the average of at least three measurements.

For analysis of the permeability as a function of elongation, it should be kept in mind that, when semicrystalline polymers are stretched, the entire film experiences deformation at lower degrees of strain. After the yield point is reached, and one region of the film is transformed to fibrous morphology, the stress becomes constant, as does the degree of deformation in the regions of the film which do not experience plastic deformation. As a result, the data presented in *Figures 7–10* are plotted using two strain axes. The top axis provides the degree of strain experienced by the entire specimen, while the bottom axis denotes the local

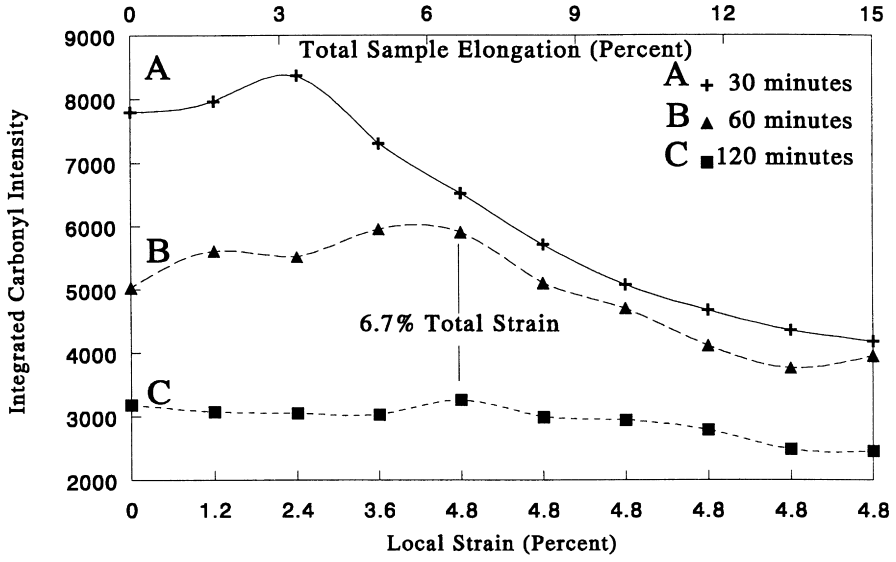

Figure 9 Integrated intensity of the band at 1768 cm^{-1} plotted as a function of elongation. Data obtained from PVDF of 150 000 MW, experiencing elastic deformation. Curves A, B and C represent films dried 30, 60 and 120 min prior to elongation, respectively

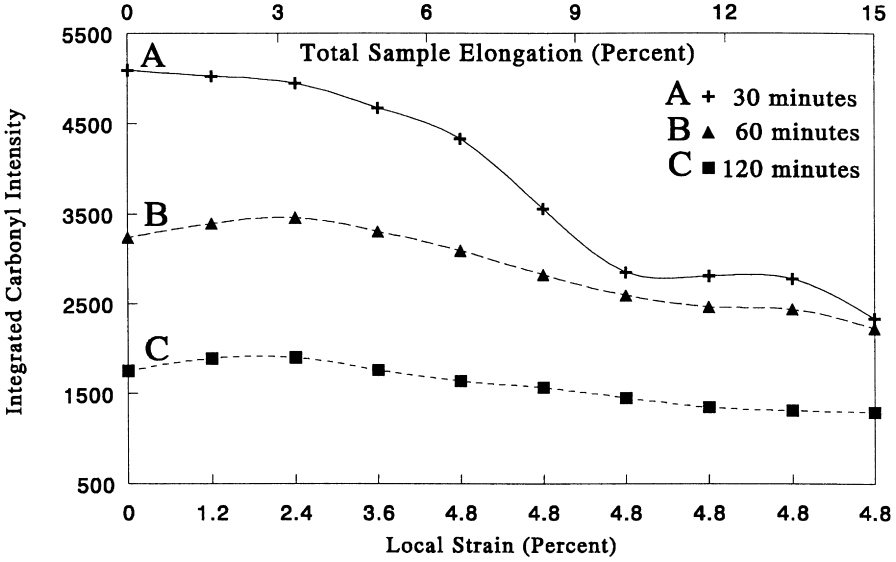

Figure 10 Integrated intensity of the band at 1768 cm^{-1} plotted as a function of elongation. Data obtained from PVDF of 350 000 MW, experiencing elastic deformation. Curves A, B and C represent films dried 30, 60 and 120 min prior to elongation, respectively

extent of deformation in the region of the film being examined.

Analysis of the data shown in *Figures 7–10* indicates that, in all cases, the amount of EtAc that diffuses to the vapour phase depends upon the length of time allowed for PVDF specimens to dry prior to the experiment. The specimens dried for 30 min display significantly higher vapour phase EtAc concentrations during the early stages of deformation, than the films exposed for longer times. These differences can be attributed to the fact that, after 30 min, the concentration of the diffusant molecules within the film remains high (*Figure 4*), and the amount entering the vapour phase changes rapidly with time. Allowing the specimen to dry for 60 or 120 min results in a lower initial EtAc concentration at the early stages of the experiment, as well as diminished time dependence for exudation of EtAc.

Upon elongation, similar trends are apparent in the PVDF specimens with 45 000, 59 000, and 150 000 MW (*Figures 7–9*). As we recall, as a result of increased free volume of the amorphous phase, the permeability of the films with partial spherulitic morphology is expected to increase upon elongation. Curves A in *Figures 7–9* show an increased rate of diffusion following 2.4% local strain. The continuous decrease in the rate of EtAc exudation, at local strains higher than 2.4%, is attributed to the rapidly decreasing concentration of EtAc in the film after 30 min of drying. The increased rate of EtAc diffusion due to the increased free volume of the amorphous phase at higher elongations is offset by the declining concentration of EtAc in PVDF. Therefore, a decreased rate of EtAc exudation at strains greater than 2.4% local strain is observed, despite the expected increase in amorphous phase free volume.

Evidence for the increased free volume at higher local strains can be observed in curves B and C in *Figures 7–9*. Upon increase of local strains for initial local strains not exceeding 4.8%, each specimen exhibits increased permeability. The 45 000 and 150 000 MW PVDF specimens achieve local strains of 4.8%, while the 59 000 MW

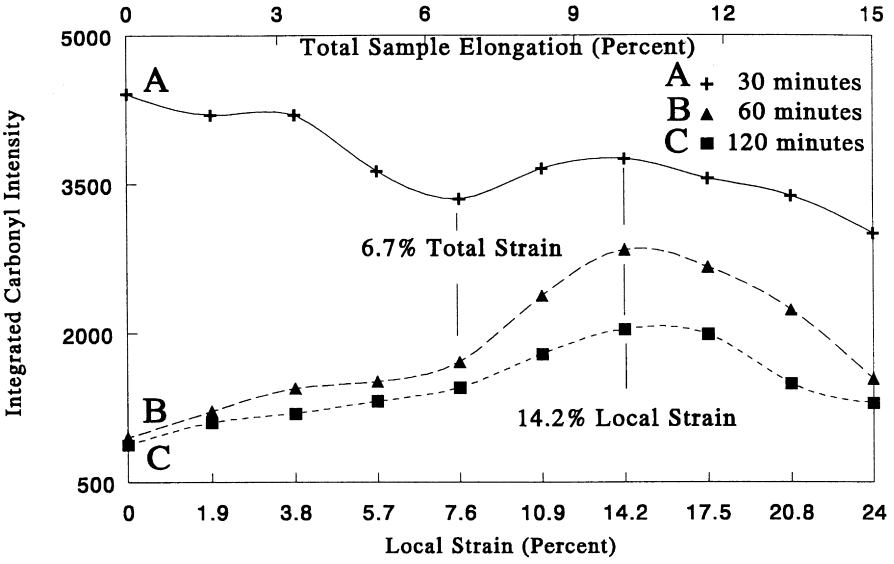

Figure 11 Integrated intensity of the band at 1768 cm^{-1} plotted as a function of elongation. Data obtained from PVDF of 45 000 MW, experiencing plastic deformation. Curves A, B and C represent films dried 30, 60 and 120 min prior to elongation, respectively

PVDF elongates only 3.6% in the elastically deforming region. As we recall from the results in *Figure 3*, the film volume increases by less than 1% at these local strains. Using 50% crystallinity as an example, and considering the non-deformable nature of the polymer crystals, less than 1% increase of the film volume corresponds to an increase of amorphous phase specific volume by less than 2%. In spite of the decreased concentration of the diffusant in the film at that point of the experiment, this seemingly small increase in the specific volume is sufficient to result in the enhancement of the EtAc diffusion at 4.8% strain. Once the yield point is reached, and no further local morphology changes occur, the amount of EtAc diffusing from the polymer becomes dependent upon the concentration of EtAc within the film, resulting in the decreased amount of EtAc diffusing out of the network.

The changes in permeability of the 350 000 MW PVDF resulting from elastic deformation are shown in *Figure 10*. Curves B and C indicate that, up to 2.4% elongation, an increased rate of EtAc diffusion is induced by local strains. While the strain measurements indicate further deformations of this region to 4.8% local strain, the transport properties are not enhanced beyond a 2.4% local strain. This behaviour is consistent with the data presented in *Table 2*, where the decreased permeability of the film at 5% total strain (3.6% local) is observed, and it is likely attributable to the fact that, up to 2.4% local strain, the free volume of the amorphous phase increases due to the displacement of crystallites. Beyond this point, a sufficient number of tie molecules are drawn taut to hinder the freedom of motion of the amorphous phase, and thus decrease its free volume. This behaviour of a high molecular weight PVDF, and its lack for lower molecular weight PVDF, can result from the fact that the number of tie molecules depends linearly upon molecular weight[19]. Therefore, 350 000 MW PVDF should have many more tie molecules, than the lower molecular weight analogs, to be drawn taut and limit diffusion.

Let us now examine how PVDF with various molecular weights and backbone structures respond to plastic deformations. Prior to the yield point, elongation of the film results in elastic deformation along the entire length of the film. However, the narrowed region of the film (*Figure 1*) experiences greater stresses per unit area than the remainder of the film. As a result, it responds by undergoing greater elongations. The accelerated deformation of this region is reflected in the strain values on the lower *x* axis (*Figures 11–14*), which provides the scale for local strains. As we recall, the micrographs in *Figures 2* and *6*, which demonstrated that when 150 000 MW PVDF yields to an imposed uniaxial stress, and begins the transition from a spherulitic to a fibrous morphology, voids form within the film, as spherulites and lamellae are broken up, and polymer chains move to assume orientations parallel to the draw direction. Therefore, morphological transformations should correspond to significantly enhanced permeability, since voids provide unobstructed diffusion pathways.

Figures 11–14 illustrate permeability plotted as a function of elongation for the region of the film which experienced plastic deformations. Again, curves A, B and C were obtained from the specimens allowed to dry prior to deformation for 30, 60 and 120 min, respectively. As was discussed earlier for *Figures 7–10*, the relative intensities of curves A, B and C in *Figures 11–14* result from the diminished concentration of EtAc over time (*Figure 4*).

Figure 11 illustrates the integrated intensity of the C=O band, plotted as a function of local and total elongation, obtained from the plastically deforming region of 45 000 MW PVDF. As observed in curves B and C of *Figure 11*, increased permeability is detected through 6.7% total strain. Similar results were obtained for elastic deformations (*Figure 7*). The rate of diffusion increase, shown in curves B and C of *Figure 11* is, however, greater than that for the corresponding data in *Figure 7*. These observations indicate that the larger permeability changes are a reflection of the greater degree of strain in the plastically deforming region. In this case, 6.7% total strain corresponds to 7.6% local strain, as opposed to a 4.8% local strain for the regions that experienced elastic deformations. Higher permeability of the plastically deforming region is expected when a larger volume increase is induced at higher strains. As seen in *Figure 3*, 7.6% local deformation would be expected to result in an approximately 3% increase of the amorphous phase specific volume for a 50% crystalline polymer.

A comparison of the results shown in *Figures 7* and *11* also indicates a significant difference between the

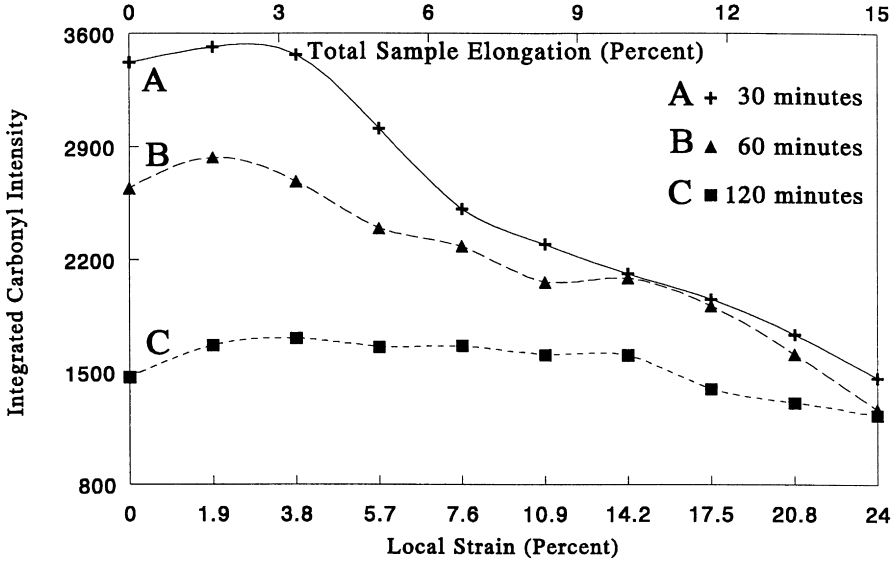

Figure 12 Integrated intensity of the band at 1768 cm^{-1} plotted as a function of elongation. Data obtained from PVDF of 59 000 MW, experiencing plastic deformation. Curves A, B and C represent films dried 30, 60 and 120 min prior to elongation, respectively

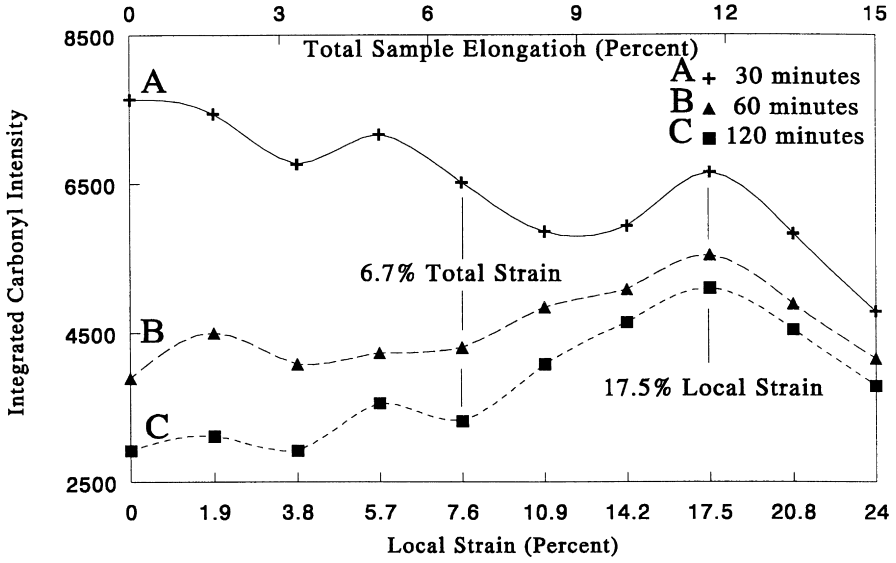

Figure 13 Integrated intensity of the band at 1768 cm^{-1} plotted as a function of elongation. Data obtained from PVDF of 150 000 MW, experiencing plastic deformation. Curves A, B and C represent films dried 30, 60 and 120 min prior to elongation, respectively

permeabilities of the elastically and plastically deforming regions of the specimen, when elongations greater than 6.7% total strain are imposed. This behaviour is attributed to the fact that, when the yield point of the polymer is passed, structural changes no longer occur in the elastically deformed regions of the film. As a result, the decreased rate of EtAc diffusion from the film observed for elastic deformation is detected (*Figure 7*), because the rate becomes dependent on the EtAc concentration within the film. However, for plastically deformed regions, void formation is observed beyond the yield point, which corresponds to 6.7% total strain, and the permeability of the film appears to increase sharply (*Figure 11*). Void formation continues to increase through a local strain of 14.2%, and parallels an increasing rate of EtAc diffusion. The number of voids in the plastically deforming region of the film reaches a maximum when the transformation of spherulitic to fibrous PVDF begins at 14.2% strain on a macroscopic scale. The maximum rate of EtAc diffusion from the specimen at 14.2% local strain occurs when the specimen volume has expanded less than 4% (*Figure 3*). As shown in *Figure 11*, at elongations greater than 14.2% local strain, the rate of EtAc entrance to the vapour phase depends upon its concentration in the film, resulting in the decreasing rate of exudation.

While the trends in permeability as a function of strain for 45 000 and 150 000 MW PVDF shown in *Figures 11* and *13*, respectively, are in agreement with trends observed in the previous studies, the results presented in *Figure 12* for 59 000 MW PVDF more closely resemble those obtained for 350 000 MW PVDF. Let us temporarily postpone their discussion and first re-visit the results for 45 000 and 150 000 MW PVDF. Curves B and C of *Figures 11* and *13* show an increased permeability through 6.7% total strain, beyond which they exhibit a rapid increase of permeability. However, while the permeability of the 45 000 MW PVDF

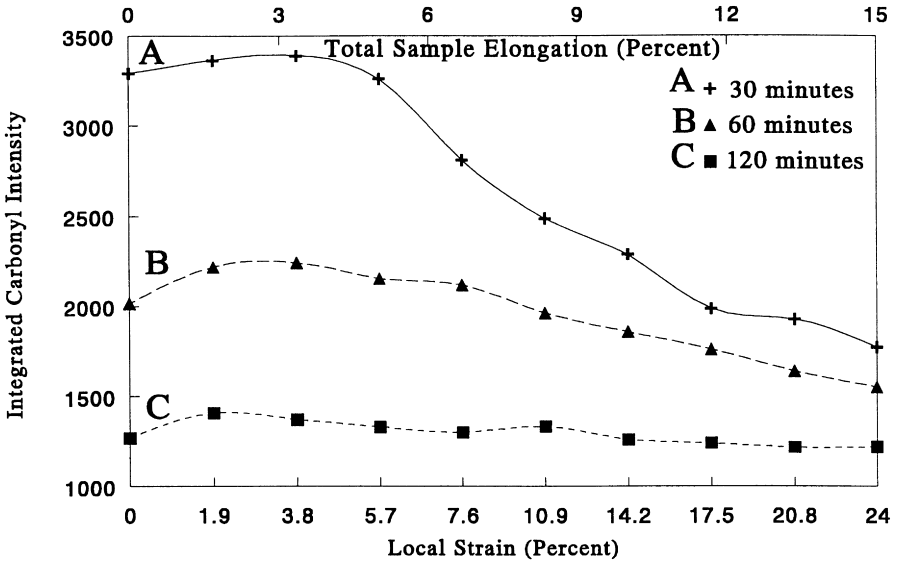

Figure 14 Integrated intensity of the band at 1768 cm^{-1} plotted as a function of elongation. Data obtained from PVDF of 350 000 MW, experiencing plastic deformation. Curves A, B and C represent films dried 30, 60 and 120 min prior to elongation, respectively

increases steadily with elongation (*Figure 11*), the 150 000 MW specimens show two apparent transitions at 1.9 and 5.7% local strains (*Figure 13*). These differences in permeability are attributed to the number and length of tie molecules connecting neighbouring crystals. Since the number of tie molecules is expected to increase linearly with MW[19], a larger number of tie molecules would be expected for 150 000 than for the 45 000 MW PVDF. Since their role in transferring stresses through a polymer system is fairly substantial, the tie molecules play a key role in the permeability changes as a function of elongation.

Based on the presented data, we are in a position to depict a scenario for the deformations and the resulting volume changes in PVDF. In the case of the 150 000 MW PVDF, the increase of the free volume, which occurs upon elongating a polymer with a spherulitic morphology, results from an increase of the volume of the amorphous phase. As crystals are drawn apart, they interfere with lateral contraction of the amorphous phase, increasing its volume. As the volume increases, conformational changes become less restricted for amorphous phase polymer chains, and the free volume increases. In order for crystals to be drawn apart, stresses must be applied, which are transferred through a semicrystalline polymer through pulled taut tie molecules. *Figure 15* presents a simplified scheme depicting the effect of tie molecules on deformation. For the sake of clarity only tie molecules are shown in the amorphous region. While *Figure 15A* illustrates the tie molecules relaxed prior to the application of stress, *Figure 15B* depicts the same crystals after sample elongation, when tie molecules have been pulled taut by the displacement of crystals from their initial positions. As a polymer film is elongated, and the crystals are drawn apart, an increased number of tie molecules are drawn taut, and cause displacement of other crystals.

The degree to which amorphous phase free volume increases, depends on the number of displaced crystals and the extent of their displacement. Owing to its relatively short chain length, 45 000 PVDF is likely to have a small distribution of tie molecule lengths. This causes all tie molecules that bridge neighbouring crystals to be drawn taut at approximately the same degree of elongation. This is shown in *Figure 15B*. This behaviour leads to a continuous

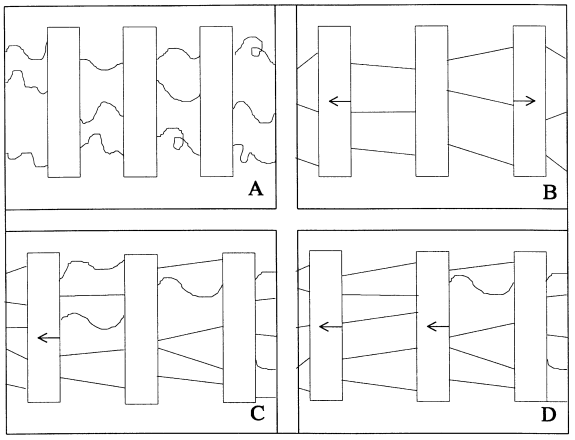

Figure 15 Schematic diagram depicting the effect of variations in tie molecule length on the deformation behaviour of PVDF

increase in the amorphous phase free volume and enhanced permeability. However, in the case of 150 000 MW PVDF, longer polymer chains may result in a larger distribution of the tie molecule lengths. During the early stages of deformation, such a condition would result in a fraction of tie molecules being pulled taut while others remain in more relaxed conformations. This behaviour is depicted in *Figure 15C*, and also explains the apparent transitions in permeability for 150 000 MW PVDF shown in *Figure 13*.

Referring again to the original dimensions of the samples in *Figure 1A*, one notes that the region of the film, which shall experience plastic strain, and from which the data in *Figure 13* was obtained, varies in width by a factor of two. The narrowed region of the sample experiences the same stresses as the remainder of the film, resulting in greater stresses per unit cross-sectional area, and greater deformations per each elongation step. The degree of strain is greater in the narrowed region than the remainder of the film, and it is also anticipated to vary over the length of the plastically deforming region. This is because relatively large changes in the specimen width occur in this region. Therefore, after the first stage of deformation, up to 1.9% local strain, the

fraction of tie molecules which have been drawn taut is expected to be highest in the narrowest segment of the specimen, and will decrease as the width of the sample increases. The degree of volume expansion that occurs in a segment of the film upon further elongation depends upon how this segment of the network responds to the applied stresses transferred though adjacent segments with different widths. If the taut tie molecules are able to resist being unfolded from their anchoring crystals, the crystals move as a unit, no increase in the amorphous phase free volume occurs between the crystals, and the volume expansions occur elsewhere within the network. If, however, there is a sufficient enhancement of the local stresses to cause partial unfolding of the tie molecules previously drawn taut, the distance between neighbouring crystals and the number of stress-bearing tie molecules will increase. This process will continue until stresses experienced by each taut tie molecule are insufficient to cause further unfolding. This is schematically illustrated in *Figure 15C* and *D*.

Thus, the rate of the free volume increase in a plastically deforming region is a complex function of the number and length of the tie molecules, their resistance to unfolding from their anchoring crystals, and the sample width. Iterative elongation steps may cause initial volume expansions in even wider segments of the specimen, or further volume increase of already deformed narrower regions. At this point, however, we are unable to establish which of these mechanisms dominates the process responsible for the local maxima in permeability observed at 5.7% local strain shown in *Figure 13*.

One of the difficulties in interpreting the data presented in *Figures 11* and *13* is the degree of strain at which the maximum rate of EtAc exudation is observed. For the PVDF specimens of 45 000 and 150 000 MW, exudation maxima of EtAc are detected at local strains of 14.2 and 17.5%, respectively. This may result from the crystallite size differences. Although the PVDF specimens exhibit similar degrees of crystallinity, as revealed by the d.s.c. measurements (*Table 1*), the crystallites of 45 000 MW PVDF are smaller than those obtained from the 150 000 MW PVDF. This is suggested by the higher permeability values of 45 000 MW samples at 0% strain (*Table 2*), as well as overall MW-crystallite size dependence discussed earlier. Typically, a smaller crystallite size and a similar degree of crystallinity result in the presence of a larger number of individual crystallites per unit volume. This behaviour would be more anticipated for 45 000 MW PVDF than for 150 000 MW PVDF. Following the formation of microcracks between neighbouring crystallites, the crystallites will continue to separate, and expand the crack, until surrounding crystallites interfere with their movement, at which point deformation will occur through the formation of new cracks. The proximity of neighbouring crystals in 45 000 MW PVDF hinders the expansion of cracks, leading to a more rapid formation of new cracks, and the spread of crazing through a larger volume of the sample. Maximum diffusion of EtAc from the film is observed when microcracks and voids have formed throughout the plastically deforming region (*Figure 1*), which occurs at 14.2% local strain for 45 000 MW PVDF, and 17.5% local strain in the case of 150 000 MW PVDF.

Let us go back to the analysis of data for PVDF of 59 000 and 350 000 MW shown in *Figures 12* and *14*, respectively. As seen, the diffusion of EtAc increases during the initial stages of deformation, followed by a decreased exudation with further elongation. The macroscopic observation, that

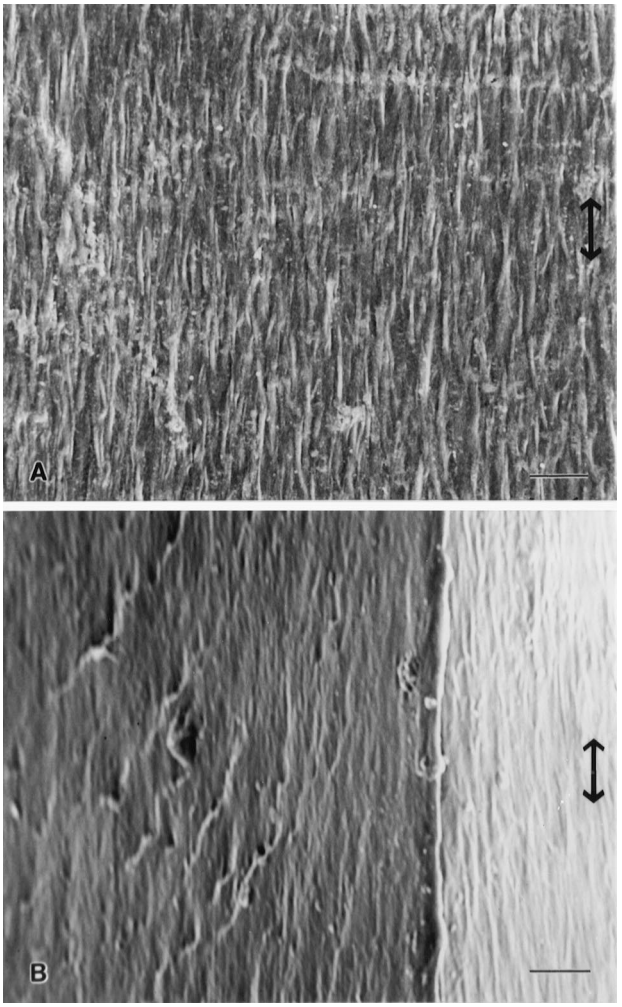

Figure 16 Scanning electron micrographs of 59 000 MW PVDF after experiencing local strains in excess of 400%: (A) film surface; (B) cross section taken near film surface

these films undergo transformation to a fibrous morphology with little whitening, suggests that the void formation still occurs, but is limited. To determine the structure of the fibrous region of these specimens, the micrographs shown in *Figure 16* were collected from the fibrous region of a 59 000 MW PVDF specimen. *Figure 16A* depicts the specimen surface, with the fibres parallel to the direction of applied strain. These results agree with those obtained for the 150 000 MW PVDF specimen (*Figure 6B*). The fractured cross section of the 59 000 MW PVDF specimen, shown in *Figure 16B*, also exhibits the fibrous structure seen on the film surface. A comparison of the cross sections of the 59 000 (*Figure 16B*) and 150 000 (*Figure 6A*) MW PVDF reveals a significant difference between the specimen morphology. The cross section of the 59 000 MW PVDF appears nearly continuous, with the presence of only a few voids. The cross section of the 150 000 MW PVDF exhibits a great deal of texture, which is attributed to the presence of a large number of voids in the specimen prior to fracture. Analysis of the micrographs presented in *Figure 16* shows that, while the 59 000 MW PVDF specimen does take on a fibrous morphology upon uniaxial elongation, the process does not involve the creation of a significant number of voids in the network. The failure of these specimens to exhibit extensive void formation during their transformation to the fibrous morphology, combined with the relatively low

Table 3 Stress–strain data acquired from the specimens examined in this study

Molecular weight	HHTT defects (%)	Young's modulus E (N mm^{-2})	Yield strength σ_y (N mm^{-2})
45 000	9–10	7.8 ± 0.2	41.8 ± 2.0
59 000	11–12	4.6	36.6
150 000	9–10	7.4	45.7
350 000	11–12	5.5	36.7

degree of strain at which the maximum rate of EtAc diffusion is achieved, indicates that the formation of a large number of voids in the network is a key feature for maximum permeability. Therefore, before continuing further analysis of the 59 000 and 350 000 MW specimens, let us identify the factors which contribute to the void formation during uniaxial elongation.

Microcracks and voids are formed when neighbouring crystals move apart. In order for the crystals to be displaced, stresses must be applied to them by taut tie molecules. If the force required to displace the crystals is greater than the force required to unfold tie molecules from their anchoring crystals, limited void formation may be expected during transformation from the spherulitic to the fibrous morphology. The amount of stress required to unfold tie molecules from the crystals is anticipated to be a function of the crystal perfection. The greater the number of intermolecular interactions between the segment of the tie molecule in the crystal and the neighbouring crystalline phase, the greater the force required to cause unfolding of the tie molecule. Defects in chain structure and irregularities in the crystal lattice might be expected to reduce the number of interactions, and therefore, decrease the stress required to unfold a tie molecule from the crystal.

The melting temperature of the crystals may be also expected to be influenced by variations in the crystal size and the crystal perfection. The melting temperatures of the specimens examined in this study are presented in *Table 1*. Interestingly enough, the 59 000 and 350 000 MW PVDF specimens melt at 161°C and 163°C, respectively, while the 45 000 and 150 000 MW PVDF specimens melt at 168°C and 170°C, respectively. These data indicate that the crystals of the 59 000 and 350 000 MW specimens are less stable relative to those with 45 000 and 150 000 MW.

However, it should be kept in mind that the melting temperatures do not reflect how the crystalline phase stability is affected by external stresses. Therefore, in order to determine the effect of crystal stability on the response of the specimens to deformations, independent stress–strain experiments were performed. *Table 3* lists the values of the Young's modulus (E) and yield strength (σ_y), obtained from the specimens examined in this study. The 45 000 and 150 000 MW PVDF specimens have σ_y values of 41.8 and 45.7 N mm^{-2}, while the σ_y values of the 59 000 and 350 000 MW PVDF specimens are 36.6 and 36.7 N mm^{-2}. These data indicate that greater force is required to pull tie molecules from the crystals formed by the 45 000 and 150 000 MW PVDF, relative to the 59 000 and 350 000 MW PVDF. This suggests that the crystals of 45 000 and 150 000 MW specimens have a greater number of intermolecular interactions with the embedded tie molecule segments, which indicates the presence of fewer defects in the crystals. The stability of the crystals is also reflected in the E values. 45 000 and 150 000 MW PVDF exhibit E values of 7.77 and 7.39 N mm^{-2}, while the E values of 59 000 and 350 000 MW PVDF are 4.58 and 5.46 N mm^{-2}, respectively (*Table 3*). The greater resistance to deformation of the specimens with the lower defect content suggests that the tie molecules pulled taut in the early stages of deformation are more likely to resist being pulled from their anchoring crystals.

In addition to the stability of the crystals, one may argue that the E and σ_y values of the specimens depend upon the number of tie molecules in the network. While this issue is most certainly the case, the number of tie molecules does

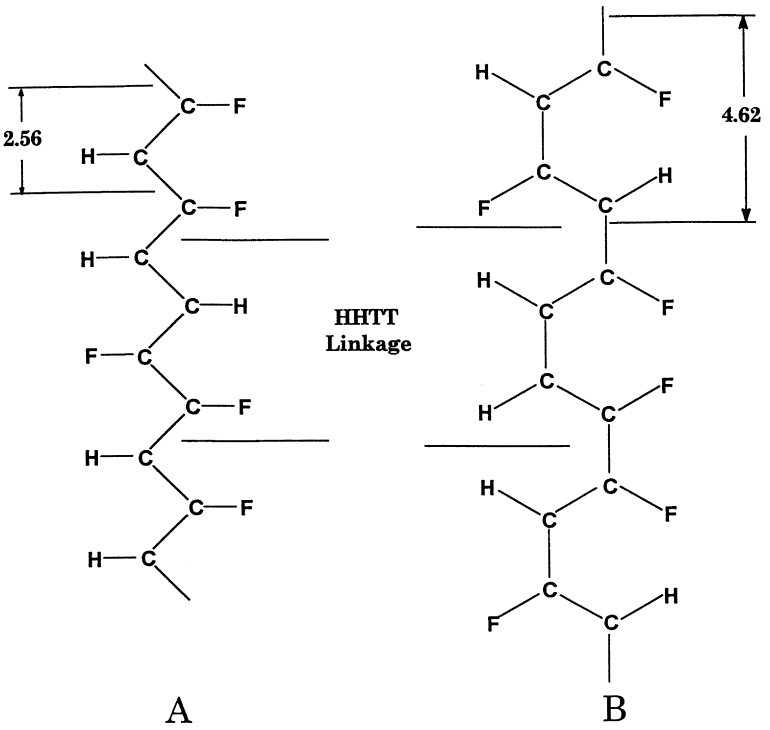

Figure 17 Conformation of PVDF in the β (A) and α (B) crystalline phases. Each F and H represent two F or H atoms. (Drawn after Ref. 13)

not play a significant role in the E and σ_y values, because 45 000 MW PVDF, which is expected to have the smallest number of tie molecules, exhibits a greater σ_y (41.8 N mm^{-2}) than the 350 000 MW PVDF (36.7 N mm^{-2}), for which the highest number of tie molecules is anticipated.

According to the data presented in *Table 3* and experimental evidence, it appears that there is a correlation between the void formation in the network and the σ_y and E values observed during the transition from the spherulitic to a fibrous morphology. 45 000 and 150 000 MW PVDF exhibit high σ_y and E values (*Table 3*) and the formation of a large number of voids during the transformation from the spherulitic to a fibrous morphology, while 59 000 and 350 000 MW PVDF exhibit relatively little void formation, and significantly lower σ_y and E values. These data suggest that stresses applied to the 59 000 and 350 000 PVDF cause the tie molecules to be pulled from the crystals, before the crystals experience adequate stress to result in displacement sufficient to cause microvoid and crack formation.

One issue that may result in the decreased perfection and lower stability of the crystals in 59 000 and 350 000 MW PVDF is the number of defects in the polymer chain. As was shown in *Table 1*, the 59 000 and 350 000 MW specimens contain more HHTT defects than the 45 000 and 150 000 MW specimens. Although one would not anticipate that significant changes in the crystal stability may be caused by relatively small differences in the number of HHTT defects, their effect on crystallization behaviour of PVDF should not be ignored. As indicated in the Introduction, upon cooling from the melt, PVDF is expected to crystallize in the α crystalline form. However, PVDF with an excessive concentration of HHTT defects crystallizes in the β crystalline form. Lovinger *et al.*[14] demonstrated that when PVDF with 11.4 mol% defects was quenched from the melt, the α crystalline phase was the dominant feature. A 14 mol% HHTT defect content was sufficient for PVDF to crystallize in the β phase.

Figure 17 schematically depicts how the presence of HHTT defects may affect chain conformation of PVDF. Each F and H in *Figure 17* represents the superposition of two fluorine or hydrogen atoms. The fact that HHTT defects would lead to preferential crystallization of PVDF in the β phase results from the relative van der Waals radii of F (1.35 Å) and H (1.1–2 Å). As seen in *Figure 17A*, the presence of HHTT defects in the polymer chain should have a relatively small impact on all *trans* chain conformations. This is primarily due to the difference in van der Waals radii of F and H. However, for TGTG′ conformations, shown in *Figure 17B*, introduction of HHTT defects would result in F atoms being 2.31 Å apart. Since twice the van der Waals radius of F is 2.70 Å, the presence of HHTT defects should decrease the possibility of α phase crystallization. When the chains assume TT chain conformations, which is characteristic of the β crystalline phase, they disrupt the α phase. Therefore, a reduction in polar intermolecular interactions between the nucleophilic F and electrophilic H atoms will occur, and lower the stability of the crystals. This issue is particularly relevant for 59 000 and 350 000 MW PVDF.

CONCLUSIONS

RPA *FT*i.r. spectroscopy was demonstrated to provide quantitative means of obtaining diffusion coefficients for PVDF specimens with various molecular weights under constant stresses. The sensitivity of the photoacoustic technique to species in the gas phase makes it an ideal tool suited for determination of desorption diffusion coefficients, while using volatile diffusants as a probe of network permeability. Furthermore, RPA *FT*i.r. spectroscopy is also capable of determining relative changes in permeability as a function of specimen elongation.

The strain dependent permeability in PVDF is affected by molecular weight and chain defect content in the following ways: (1) molecular weight affects the size of individual crystals of the crystalline phase and has a significant effect on the PVDF permeability; (2) the increased number of tie molecules in the network for higher molecular weight PVDF changes the network permeability upon application of external stresses; (3) while PVDF with 45 000, 59 000 and 150 000 MW exposed to 5% deformation exhibit increased permeability, the increased content of taut tie molecules in the amorphous phase for 350 000 MW PVDF results in a decrease in permeability; (4) the number of chain defects in PVDF polymer chains has a significant influence on plastic deformations. PVDF specimens with the 9–10% HHTT chain defect content exhibit yield strengths of $>$40 N mm^{-2}, while the specimens with 11–12% chain defect content yield at approximately 37 N mm^{-2}.

ACKNOWLEDGEMENTS

Acknowledgement is made to the Donors of The Petroleum Research Fund, administrated by American Chemical Society, for partial support of this research (ACS-PRF# 29083-AC7). The authors are thankful to Kathy Iverson of the Electron Microscopy Center at North Dakota State University for her valuable assistance in obtaining electron microscopy images.

REFERENCES

1. Hsu, T. C. and Geil, P. H., *J. Appl. Phys.*, 1984, **56**, 2404.
2. Hsu, T. C. and Geil, P. H., *J. Mater. Sci.*, 1989, **24**, 1219.
3. Mancarella, C. and Martuscelh, E., *Polymer*, 1977, **18**, 1240.
4. Takahashi, Y., Zakoh, T. and Hanatani, N., *Coll. Polym. Sci.*, 1991, **269**, 781.
5. Matsushige, K., Nagata, K., Imada, S. and Takemura, T., *Polymer*, 1980, **21**, 1391.
6. Siesler, H. W., *J. Poly. Sci.: Poly. Phys. Ed.*, 1985, **23**, 2413.
7. Sessler, G. M., *J. Accoust. Soc. Amer.*, 1981, **70A**, 596.
8. Lovinger, A. J., in *Developments in Crystalline Polymers*, ed. D.C. Basset. Applied Science Publishers, New Jersey, 1981, p. 48.
9. Lovinger, A. J., *Macromolecules*, 1982, **15**, 40.
10. Ludwig, B.W. and Urban, M. W., *Polymer*, 1992, **33**, 3343.
11. Ludwig, B.W. and Urban, M. W., *Polymer*, 1993, **34**, 3376.
12. Ludwig, B.W. and Urban, M. W., *Polymer*, 1994, **35**, 5130.
13. Lando, J. B. and Doll, W. W., *J. Macromol. Sci.: Phys.*, 1968, **B2**, 205.
14. Lovinger, A. J., Davis, D. D., Cais, R. E. and Kometani, J. M., *Polymer*, 1987, **28**, 617.
15. Welch, G. J. J., *Polym. Sci.: Phys. Ed.*, 1976, **14**, 1683.
16. Crank, J. and Park, G. S., *Diffusion in Polymers*. Academic Press, New York, 1969.
17. Mirkin, M.A., *Poly. Sci. U.S.S.R.*, 1989, **A31**, 404.
18. Ergoz, K., Gatou, J. G. and Mandelkern, L., *Macromolecules*, 1972, **5**, 147.
19. Lustiger, A. and Markham, R. L., *Polymer*, 1983, **24**, 1647.
20. Peterlin, A., Morphology, in *Encyclopedia of Polymer Science and Engineering*, 3rd edn., Wiley & Sons 1986, p. 281.
21. Nakagawa, K. and Ishida, Y. J., *Polym. Sci.: Polym. Phys.*, 1973, **11**, 2153.
22. Woodward, A. E., *Atlas of Polymer Morphology*. Hanser, New York, 1989.